Available online at www.sciencedirect.com
ScienceDirect
Journal of Power Sources 171 (2007) 754–762
JOURNAL OF POWER SOURCES
www.elsevier.com/locate/jpowsour

PEM fuel cell model representing steady-state, small-signal and large-signal characteristics

P.J.H. Wingelaar*, J.L. Duarte, M.A.M. Hendrix

Department of Electrical Engineering, Electromechanics and Power Electronics Group (EPE), Eindhoven University of Technology, Den Dolech 2, im 0.02, P.O. Box 513, 5600 MB Eindhoven, The Netherlands

Received 12 June 2006; received in revised form 23 May 2007; accepted 3 June 2007
Available online 13 June 2007

Abstract

Fuel cell applications become increasingly attractive. Therefore, comprehensive models, simulation software and analysis tools are required to characterize fuel cell behavior. This paper introduces a model capable of representing the static and dynamic (dynastatic) behavior of PEM fuel cells. The model approximates the theoretical current–voltage description with an equivalent electric circuit. The parameter values of the model are found by analyzing small-signal measurement results from electrochemical impedance spectroscopy, together with the steady-state electric characteristic and large-signal behavior from step-response measurements. Because the modeling approach is completely based on measurements on the fuel cell electric output terminals, electrochemical aspects like temperature dependency, charge double layer and adsorption effects are implicitly covered.

Keywords: Polymer electrolyte membrane fuel cell (PEMFC); Impedance spectroscopy; Interrupted current; Steady-state; Dynamics; Models

1. Introduction

Fuel cell applications become increasingly attractive, because they are efficient, clean, and, in the case of a polymer electrolyte membrane (PEM) fuel cell, light weighted electricity generators [1–9]. Because the interest in fuel cells grows, the urge for accurate simulation models grows as well.

The focus of the analysis and modeling of fuel cells has always been on steady-state behavior. However, fuel cells are low voltage, high current electricity generators, which is not practical in common applications. By using power electronics to convert the low voltage to a more efficient high level, one will introduce step currents, and other dynamics in the output of the fuel cell, which can certainly not be modeled by one of the two known steady-state models presented in the literature [2–9].

In the literature a transient model based on operation temperature changes was already described [4]. A major disadvantage of that model is that it requires temperature measurements. Commercial available fuel cells stacks are not always equipped with (enough) temperature sensors. However, it is possible to characterize the fuel cell dynamics also by applying step load changes [9,10] or small current variations at the output terminals [9–12]. Unfortunately, no qualitative nor quantitative comparison between both approaches can be found in the literature.

This paper presents three measurement methods (Section 2) and accompanying test results (Section 3), namely electrochemical impedance spectroscopy for small-signal behavior, steady-state measurements to determine the current–voltage characteristic and step-response to characterize large-signal behavior. A unique equivalent circuit model based on these three measurement sets is introduced in Section 3, and is validated in Section 4. This model is capable of simulating static and dynamic fuel cell behavior (a so-called "dynastatic" model) and, because this model is completely based on electrical measurements of the output terminals, it implicitly covers temperature effects, charge double layer and adsorption dynamics.

2. Method and materials

The fuel cell voltage, V_{FC}, can be expressed as a function of the fuel cell current I_{FC} [8–10]

$$V_{FC} = E_{ocv} - A \ln\left(\frac{I_{FC}}{I_0}\right) R^{int} I_{FC} + B \ln\left(1 - \frac{I_{FC}}{I_l}\right) \quad (1)$$

* Corresponding author. Tel.: +31 40 247 3554; fax: +31 40 243 4364.
E-mail addresses: p.j.h.wingelaar@tue.nl (P.J.H. Wingelaar), j.l.duarte@tue.nl (J.L. Duarte), m.a.m.hendrix@tue.nl (M.A.M. Hendrix).

0378-7753/$ – see front matter © 2007 Elsevier B.V. All rights reserved.
doi:10.1016/j.jpowsour.2007.06.001

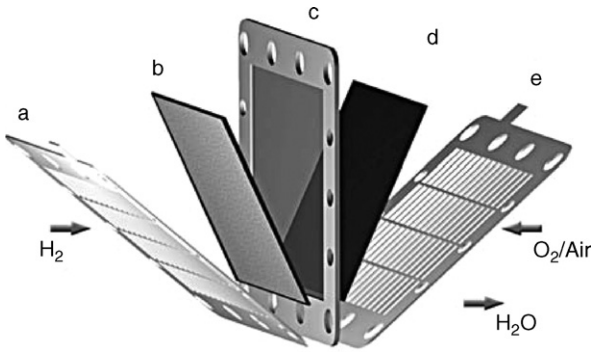

Fig. 1. Schematically drawn PEM fuel cell, with (a) the anode separator plate, (b) the anode with a carbon-based diffusion layer and platinum catalyst, (c) is the polymer electrolyte, (d) is the cathode with a carbon-based diffusion layer and platinum catalyst and (e) the cathode separator plate.

in which E_{ocv} is the open circuit voltage of the electrochemical reactions. Furthermore, three loss terms are included in (1). The first is the activation loss, which models the slowness of the reaction at the surface of the electrodes and is characterized by parameters A, the activation coefficient, and I_0, the exchange current. The second loss term is the internal resistance R^{int}, which models the ohmic losses in the conductors and the membrane. The third term is the concentration loss, which models the limit of the fuel flow to the active area of the membrane. The concentration loss is characterized with B, the concentration coefficient, and I_l, the limiting current.

From the mechanical construction of a PEM fuel cell, shown in Fig. 1, one can imagine that two ideally polarized metal plates separated by a thin plastic sheet act as a capacitor. In case of the PEM fuel cell, the large-signal dynamics of the system can be modeled using a capacitor in combination with a parallel resistor and a series resistor [8]. However, a fuel cell is an electrochemical device, and the referred capacitance is caused by a charge buildup between two different materials such as the electrode and electrolyte. As is shown in Fig. 1, a fuel cell contains two electrode–electrolyte interfaces, namely the anode–membrane and the cathode–membrane interface. Therefore, it may be expected that a fuel cell suffers from two charge double layer capacitances, resulting in two time constants [13].

Moreover, the platinum catalyst used to speed up the anode and cathode reactions, may result in an adsorption time constant [13–15,10]. This can be explained by the fact that hydrogen adsorbs to the platinum catalyst surface, as a result of hydrogen ion discharge. Hydrogen has the property to transfer directly almost completely its electron charge to the catalyst [16], resulting in an immediate voltage response, while the current of the system, e.g. the transport of protons and electrons, is not directly influenced, because the proton transport through the membrane is slow. This phenomenon creates a phase shift between current and voltage, hence, an additional time constant [9,10].

We performed three types of measurements on the fuel cell. First, impedance spectroscopy finds the small-signal response of the fuel cell in certain DC set-points. Second, steady-state measurements are done to determine the voltage–current characteristic and the maximum power rating of the fuel cell. Last, step-responses reveal the large-signal behavior of the fuel cell.

The fuel cell used for the measurements is 1 of the 12 cartridges from a commercially available 500 W fuel cell system [17,18]. The cartridge contains four membranes stacked in pairs. For the experiments, one cartridge is used and the two pairs of membranes are connected in series to increase the output voltage and limit the output current. The cartridge is mounted on a aluminium frame with a fan, which provides the oxygen to the cathode of the fuel cell. The fuel cell in this test-setup delivers a maximum output power of only 7 W due to insufficient airflow supply.

To perform the measurements, the fuel cell is coupled to a linear regulator, which is controlled by a digital signal processor [10,9]. The voltages over the drain and source of the regulator, and the current of the fuel cell are recorded by 12 bit non-multiplexed AD converters. The accuracy of the digitally measured voltages and currents is limited by the bit-error of the used converters.

3. Results

3.1. Electrochemical impedance spectroscopy

Electrochemical impedance spectroscopy (EIS) is a method to characterize electrical properties of materials and their interfaces with electronically conducting electrodes [13]. The measurement procedure is to excite the output terminals of a fuel cell at a fixed DC set-point with superimposed small amplitude sinusoidal signal. The complex impedance can be interpreted as an electrical circuit containing resistors, capacitors and inductors. Each time-constant is a result of a chemical, physical or electrochemical phenomenon.

The impedance spectroscopy measurement results carried out on the fuel cell stack are shown in Fig. 2. The frequency ranges from 0.01 Hz (right side of the semi-circles) to 45 Hz (left side of the semi-circles), and the DC-currents were set to 1, 2, 3, 4, 5 and 6 A.

In Fig. 2, the averaged data-points obtained from the measurements are shown. The test is repeated 10 times for all frequencies and for all DC points. The data is converted to the frequency-domain using a fast Fourier transform.

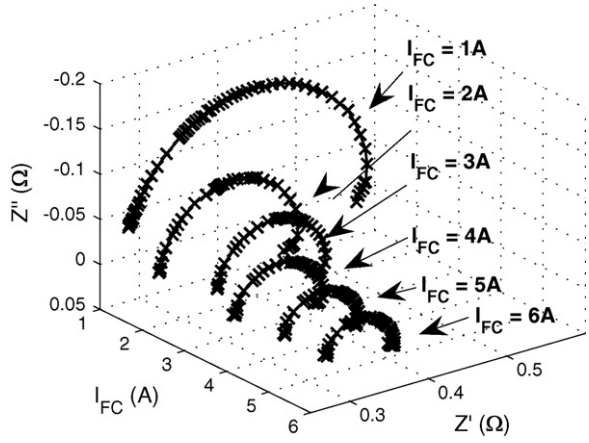

Fig. 2. Impedance plots of the fuel cell in a range from 1 to 6 A. Z' and Z'' are the measured real and imaginary impedance components, respectively.

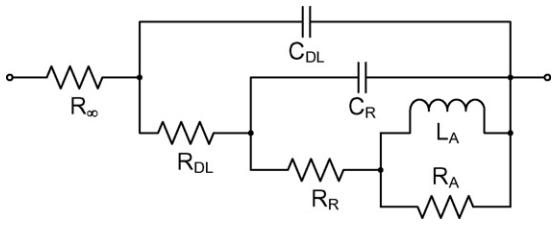

Fig. 3. Third-order ladder network for fitting impedance spectroscopy data.

The measured impedance show a large capacitive semi-circle in the frequency range of 0.1–45 Hz, which is caused by charge double layer effects. Furthermore, inductive behavior is seen in the low-frequency range, which is the right side of the impedance semi-circles. References in the literature indicate that this behavior is probably caused by the adsorption of hydrogen to the platinum surface [14,15,10].

The measurement results of the electrochemical impedance spectroscopy show inductive and capacitive behavior, which implicates that the equivalent electrical impedance should contain at least one capacitor and one inductor. The proposed equivalent impedance circuit, with two double layer capacitors C_{DL} and C_R and one adsorption inductor L_A, is shown in Fig. 3. A previous publication indicates that the fuel cell stack used is best represented with a third-order equivalent circuit model [9].

The the non-linear least-squares fit provides an accurate description of both the amplitude and the phase-shift. The values of the equivalent model are presented in Table 1.

The resistors found with EIS are graphically represented in Fig. 4. It is clear that the bulk resistor R_∞ has a constant character, and can therefore be approximated as a constant with value $R_\infty = 0.272\ \Omega$. The adsorption resistor R_A tends to slowly decrease with increasing current set points. Therefore, this resistor is approximated using

$$R_A(I_{FC}) = R_A^0 - \alpha_A I_{FC}, \tag{2}$$

where $R_A^0 = 23.5\ \text{m}\ \Omega$ represents the initial value and $\alpha_A = 2.62\ \text{m}\ \Omega\ \text{A}^{-1}$ is the linear coefficient.

The two double layer resistors (R_{DL} and R_R) are showing non-linear behavior dependent on the fuel cell current. From Joule's law, it follows that the temperature dependency of a conductor is proportional to the square of the current through the conductor, that is,

$$T \propto I_{FC}^2. \tag{3}$$

Therefore, in first approximation a function representing the resistors is proposed as being proportional to the square of the fuel cell output current. The implementation of the resistor functions is

$$R_{DL}(I_{FC}) = R_{DL}^\infty + R_{DL}^0 e^{-\alpha_{DL}^* I_{FC}^2}, \tag{4}$$

and

$$R_R(I_{FC}) = R_R^\infty + R_R^0 e^{-\alpha_R^* I_{FC}^2}. \tag{5}$$

The settling value for the first double layer resistor is $R_{DL}^\infty = 75.2\ \text{m}\ \Omega$, which represents the resistance for large output currents (I_{FC}). Furthermore, the initial value $R_{DL}^0 = 172\ \text{m}\ \Omega$ and the exponential rate coefficient $\alpha_{DL}^* = 0.342\ \text{A}^{-2}$. The second double layer resistance is characterized with $R_R^\infty = 18.4\ \text{m}\ \Omega$, $R_R^0 = 97.0\ \text{m}\ \Omega$ and a rate coefficient $\alpha_R^* = 0.244\ \text{A}^{-2}$. The fit is presented in Fig. 4(a).

However, from the measurement data presented in Fig. 4, the exact characteristic of the double layer resistors cannot be determined in the low current region. This is due to the limitations of the measurement-setup to measure the injected small current variations so that the obtained voltage variations are undistort.

A second approach assumes that the temperature changes are small. In that case, the current–temperature relationship (3) can be linearized, resulting in

$$T \propto I_{FC}. \tag{6}$$

Using this linear relationship, the resistor functions can be represented with

$$R_{DL}(I_{FC}) = R_{DL}^\infty + R_{DL}^0 e^{-\alpha_{DL} I_{FC}}, \tag{7}$$

$$R_R(I_{FC}) = R_R^\infty + R_R^0 e^{-\alpha_R I_{FC}}. \tag{8}$$

The values for the first double layer resistor are $R_{DL}^\infty = 67.8\ \text{m}\ \Omega$, $R_{DL}^0 = 313\ \text{m}\ \Omega$ and the exponential rate coefficient, $\alpha_{DL} = 0.884\ \text{A}^{-1}$. The values for the second double layer resistor are $R_R^\infty = 15.3\ \text{m}\ \Omega$, $R_R^0 = 199\ \text{m}\ \Omega$ and the rate coefficient, $\alpha_R = 0.907\ \text{A}^{-1}$. The fits are presented in Fig. 4(b).

The EIS data also provides an indication of the values for the double layer capacitances and adsorption inductance. Literature indicates that these elements have constant values [16,13]. Fig. 5 shows the values for the double layer capacitances (◯-mark for C_{DL} and ●-mark for C_R) and the adsorption inductance L_A (□-mark).

Table 1
Parameter values of the third-order equivalent circuit model of the PEM fuel cell based on the data from electrochemical impedance spectroscopy

	DC set-points					
	1 A	2 A	3 A	4 A	5 A	6 A
$R_\infty(\Omega)$	0.283	0.270	0.290	0.257	0.266	0.265
C_{DL} (F)	0.221	0.259	0.263	0.243	0.229	0.226
$R_{DL}(\text{m}\Omega)$	202	107	107	82.3	65.7	64.5
C_R (F)	0.450	0.364	0.745	0.691	0.566	0.795
$R_R(\text{m}\Omega)$	92.3	54.9	18.1	21.7	24.2	18.2
L_A (mH)	36.0	45.3	37.3	35.3	38.5	48.4
$R_A(\text{m}\Omega)$	19.1	20.4	16.6	12.3	9.37	8.2

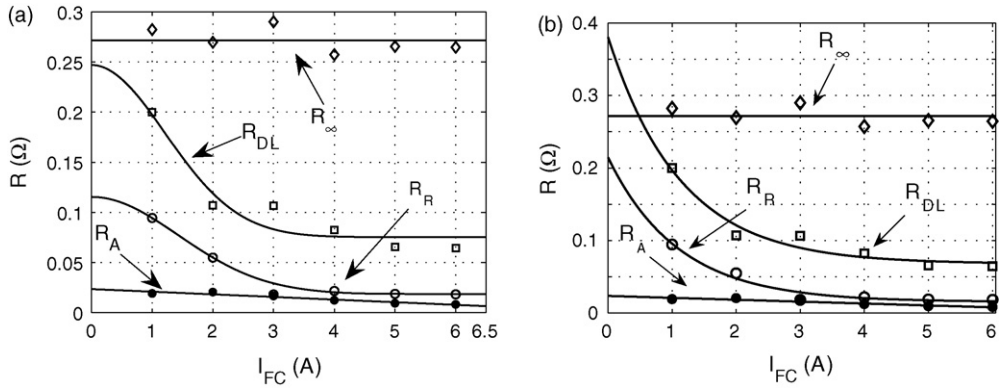

Fig. 4. Resistor values found with impedance spectroscopy and their fitted function results. In (a) a quadratic and in (b) a linear relationship between the fuel cell current and operating temperature is used.

From Fig. 5, it is clear that the first double layer capacitor $C_{DL} = 0.241$ F and the adsorption inductor $L_A = 40.2$ mH can be interpreted as constants. The second double layer capacitor (C_R), however, can hardly be assumed as constant.

The second double layer capacitor is more difficult to fit in the higher DC current region, because the semi-circle in the complex impedance plane as the result of the parallel circuit R_R and C_R is dependent on the value of the second double layer resistor R_R. Because this resistor becomes small at higher output currents, the amplitude of the semi-circle also becomes small.

3.2. Steady-state characteristic

Steady-state measurement results are presented as ◯-marks in Fig. 6. The characteristic shows almost no concentration polarization, which can be interpreted as the concentration coefficient that goes to zero, ($B \rightarrow 0\,V$) [10,9]. As a consequence, the expression for the fuel cell voltage (1) may be simplified to

$$E_{FC} = E_{ocv} - A \ln\left(\frac{I_{FC}}{I_0}\right) - R^{int} I_{FC}. \quad (9)$$

The theoretical value of the reversible voltage of a single cell is 1.229 V under standard conditions (that is for temperatures of 25 °C and standard pressure of the reactants). However, because literature indicates that the standard operating temperature of a PEM fuel cell is around 60 °C [8–10], and because the reversible cell voltage is dependent on the operating temperature [8,4,9,10], the reversible cell voltage is calculated to be $E_{rev} = 1.17$ V. As was indicated in Section 2, the used fuel cell stack contains four membranes in series, resulting in a theoretical open circuit voltage of

$$E_{ocv} = 4E_{rev} = 4.68. \quad (10)$$

With the values for the different resistors known, the steady-state resistance R^{int} can be determined. Because in steady-state operation the adsorption inductance L_A is short circuiting the adsorption resistance R_A, the total internal resistance, which is dependent on the output current of the fuel cell stack (I_{FC}), is determined by

$$R^{int}(I_{FC}) = R_\infty + R_{DL}(I_{FC}) + R_R(I_{FC}). \quad (11)$$

Because there are two possibilities of determining the values for the double layer resistors, the results of the open circuit voltage source, shown in Fig. 7, are also presented in two forms. Fig. 7(a) shows the open circuit voltage source (E_{FC}) of the fuel cell stack for double layer resistors presented with (4) and (5),

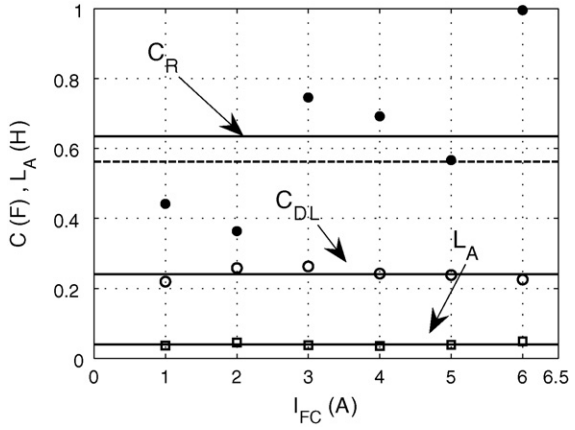

Fig. 5. Measured values and fitted as a constant (lines) of the two double layer capacitors (C_{DL} and C_R), and the adsorption inductor (L_A).

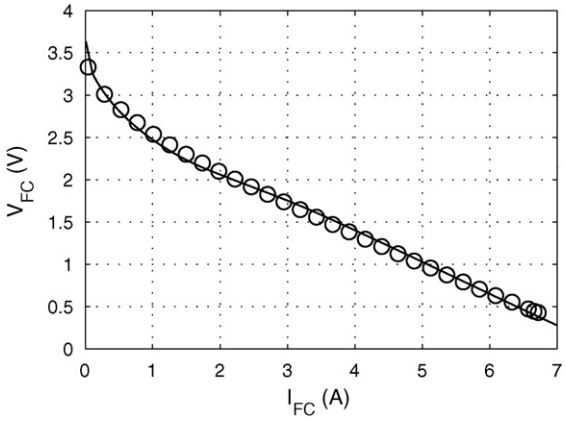

Fig. 6. Steady-state characteristic measured at the four membrane stack. The ◯-marks are the measured points, the full line is the fitted characteristic.

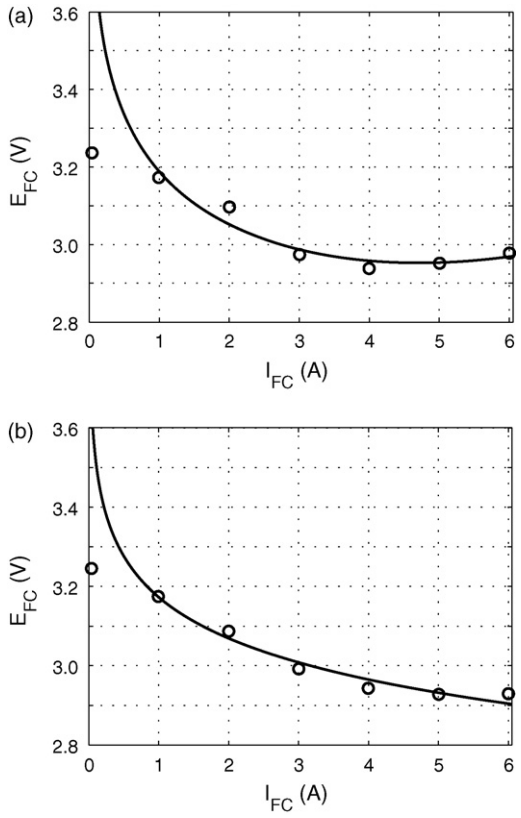

Fig. 7. Open circuit source characteristics (◯) and the fit (full line). In (a) a quadratic and in (b) a linear relationship between fuel cell current and operating temperature is used.

while Fig. 7(b) presents E_{FC} for the double layer resistors from (7) and (8).

The difference between Fig. 7(a) and (b) directly shows the problem in fitting the double layer resistors with the current temperature relationship of (3). The open circuit voltage source of the stack has a minimum value at $I_{FC} = 4$ A, while the E_{FC} in Fig. 7(b) has a continuously decreasing trend.

The large discrepancy between the first measurement point ($I_{FC} = 0$ A) and the simulated value, which can be seen in Fig. 7(b), is related to the internal current of the fuel cell [8]. This loss current prohibit the fuel cell from producing its open circuit voltage. A schematic representation of the fuel cell including the internal current source is shown in Fig. 8.

In order to decide whether assumption (3) or (6) is best, the steady-state model (10) is first fitted using the least squares method to the open circuit source of Fig. 7(a). To include the minimum in the characteristic (at $I_{FC} = 4$ A), the activation coefficient A has to be rewritten. The proposed open circuit voltage source is

$$E_{FC} = E_{ocv} - (a + bI_{FC}^2) \ln\left(\frac{I_{FC}}{I_0}\right) \tag{12}$$

where the activation coefficient is made dependent on the square of the fuel cell output current. The fit results in the constant term of activation $a = 0.216$ V, the activation resistive term $b = 541\ \mu\Omega\ A^{-1}$ and the exchange current $I_0 = 972\ \mu$A. The error made between the open circuit function (the full line of Fig. 7(a)) and the measured data points is less than 2% except for $I_{FC} = 0$ A.

Second, the kinetic mode steady-state model is fitted to the data from Fig. 7(b). For this fit, the activation coefficient A is assumed to be constant, resulting in

$$E_{FC} = E_{ocv} - A \ln\left(\frac{I_{FC}}{I_0}\right), \tag{13}$$

where $A = 0.164$ V and $I_0 = 117\ \mu$A. The error between this function (the full line of Fig. 7(b)) and the obtained data is less than 1%, except for $I_{FC} = 0$ A.

Although both solutions for the double layer resistors are applicable to find a model for the open circuit voltage source E_{FC}, solution (13) is more attractive. Not only is the error between the fitted open circuit voltage source in favor of the linear current dependency of the double layer resistors, but also the complexity of (13) is lower than that of (12).

3.3. Step-response measurements

With the step-response test, the load current of the fuel cell is suddenly changed from one value to another. This method can be useful in studying the fuel cell response to switched-mode converters, because the input of these converters would excite the fuel cell in a similar way. Step measurements fitted to a first-order model show a step polarity dependent time-constant, which is unsuited for a linear circuit model description [9,10].

By fitting the step-response to the proposed dynamic model of Fig. 9, including a constant value for C_R, the results indicate which value is to be used. The average value for all data points is $C_R = 0.634$ F (full line in Fig. 5), while the average value when omitting the last data point result in $C_R = 0.562$ F (dashed line in Fig. 5).

For the verification of these assumed constant values for the capacitors and inductor, a simulation of the step-response is made and compared with the measured characteristic. In Fig. 10, the simulated and measured voltages of the fuel cell stack are shown in response to the current delivered. The simu-

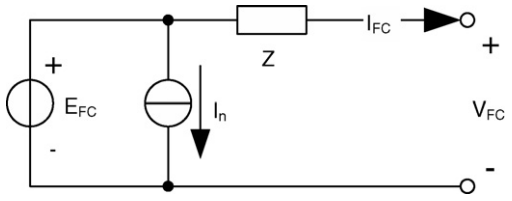

Fig. 8. Representation of the fuel cell including the internal current source I_n.

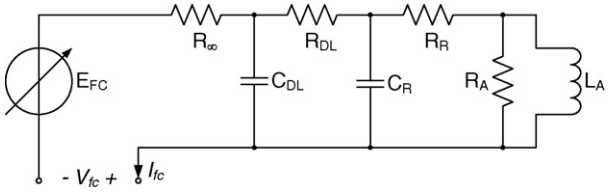

Fig. 9. Equivalent circuit model for a PEM fuel cell stack, featuring one or two double layer time-constants and an inductive adsorption time constant.

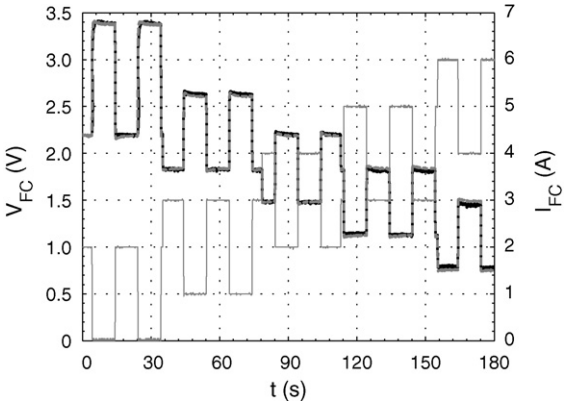

Fig. 10. Step-response: simulated voltage in Matlab (gray dashed line), measured voltage (black line) and measured current (thin gray line).

lated response is made while using $C_R = 0.562$ F for the second double layer capacitor.

The error b etween the measured and simulated step-response is calculated using both modeling possibilities for the second double layer capacitor. The difference between the response for $C_R = 0.562$ F and $C_R = 0.634$ F is marginal, that is, less than 3 mV peak and an average difference of less than 8 μV over the complete time interval. The largest voltage peaks of the error occur at the switching of the load.

The step-response simulation is made by calculating the immediate changes in the resistances caused by the change in output current (2), (7) and (8) and combining those values with the steady-state voltage source (13), except for the value of the internal voltage source when $I_{FC} = 0$ A. For that specific situation, an approximation of the internal voltage source is made, based on the value found in Fig. 7(b).

The equivalent circuit model of Fig. 9 is determined with analytical expressions listed in Table 2. For the analytical equations of the double layer resistors R_{DL}, and R_R, and for the open circuit voltage source E_{FC}, the linear relationship (6) between temperature changes and output current is used.

4. Model verification

The model, with parameters as given in Table 2, is verified with simulations in Matlab of the steady-state, small- and large-signal response, and the results are compared with the measured data. First, the electrochemical impedance data will be verified. Second, the steady-state characteristics are checked, and last, the step-response is inspected.

The definition of the error (ε) used in the verification is

$$\varepsilon = \frac{V_{FC,sim} - V_{FC,meas}}{V_{FC,meas}} \times 100\%, \tag{14}$$

and is the relative error between the simulated voltage $V_{FC,sim}$ and the measured voltage $V_{FC,meas}$ of the fuel cell.

4.1. Small-signal verification

The simulation of the frequency response of the model is done by implementing the complex impedance in Matlab. Afterwards, the calculated values of the impedance are compared to the measured ones. The relative error ε between measurement and simulation is shown in Fig. 11. The top left graph shows the model error with a DC set point of $I_{FC} = 1$ A. The top right graph shows the error for $I_{FC} = 2$ A DC setting, the middle left for $I_{FC} = 3$ A, etc.

From the figure, it can be seen that the largest deviation appears for 1 and 3 A DC set point. This can be explained by referring to Fig. 2, where the same measurements show a slight shift of the semi-circles over the real axis. This shift results in a higher measured bulk resistance R_∞ than is used for the simulation, which results in a higher relative error.

Table 2
Analytical equations and values of the fuel cell model for a four membrane PEM fuel cell stack

Model equations	Components	Values	Units
$E_{FC} = E_{ocv} - A\ln(I_{FC}/I_0)$	E_{ocv}	4.68	V
	A	0.164	V
	I_0	117	μA
R_∞	R_∞	0.272	Ω
C_{DL}	C_{DL}	0.241	F
$R_{DL} = R^\infty_{DL} + R^0_{DL}e^{-\alpha_{DL} I_{FC}}$	R^∞_{DL}	67.8	m Ω
	R^0_{DL}	313	m Ω
	α_{DL}	0.884	A^{-1}
C_R	C_R	0.562	F
$R_R = R^\infty_R + R^0_R e^{-\alpha_R I_{FC}}$	R^∞_R	15.3	m Ω
	R^0_R	199	m Ω
	α_R	0.907	A^{-1}
L_A	L_A	40.2	mH
$R_A = R^0_A - \alpha_A I_{FC}$	R^0_A	23.5	m Ω
	α_A	2.62	m Ω A^{-1}

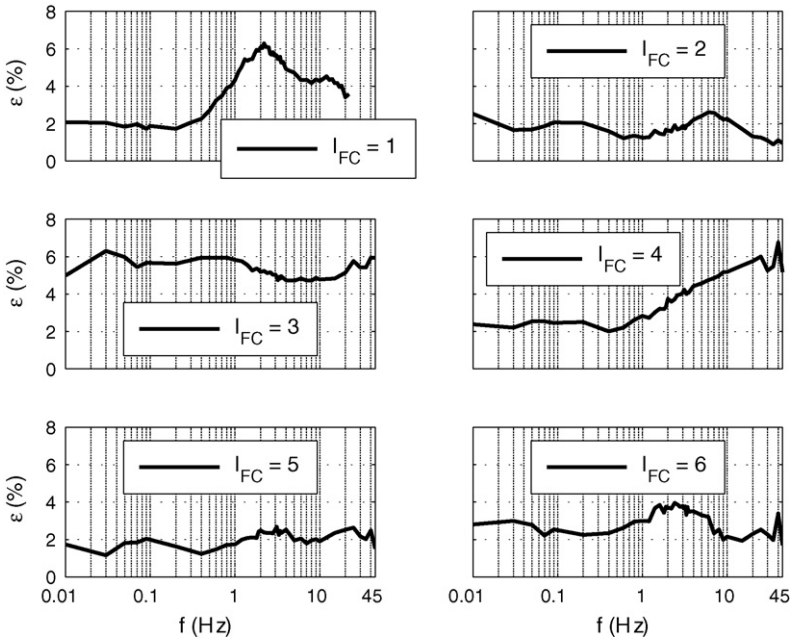

Fig. 11. Relative error between the measured small-signal characteristic of the fuel cell and the simulated characteristic, for different DC set points.

The error at $I_{DC} = 4$ A increases at higher frequencies. This effect is also related to a difference in bulk resistance compared to the used simulation value. An error in the bulk resistance will be enlarged in the higher frequency range, because the bulk resistor becomes a relatively larger part in the internal resistance of the model (R^{int}). This can be seen in the $I_{DC} = 1$ A, $I_{DC} = 3$ A and $I_{DC} = 4$ A plots.

From the results shown in Fig. 11, it can be concluded that the average error made in the small-signal behavior is lower than 4%. The peak error is 6%.

4.2. Steady-state verification

The error (ε) made in the steady-state simulation is presented as the ◯-marks connected with the dotted line in Fig. 12. As predicted, the error between the measured output voltage at $I_{FC} = 0$ A deviates most. The other verified points are very close to the obtained values, and the error differs at most 3% (at $I_{FC} = 6$ A).

To reduce the error at very low output currents of the stack, the steady-state equation (13) is expanded with an internal current term I_n, as proposed in reference [8]. The values for the open circuit voltage source (E_{FC}) are fitted to

$$E_{FC} = E_{ocv} - A \ln\left(\frac{I_{FC} + I_n}{I_0}\right), \tag{15}$$

and for the new expression the parameters change to $A = 193$ mV, $I_0 = 631$ μA and the fuel crossover or internal current term will be $I_n = 470$ mA. The fuel cell stack is made from four membranes with an active area of $A_e = 60\,cm^2$ each, which leads to an internal current density of $j_n = 2\,mA\,cm^{-2}$. This value is marked in the literature as "normal" [8].

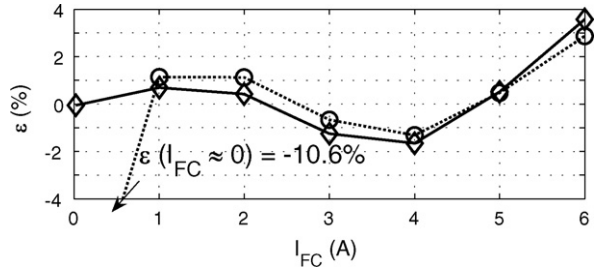

Fig. 12. Relative error between the measured and the simulated steady-state characteristic.

The results of the steady-state verification using the internal current lead to the error plot with the full line and the ◊-marks of Fig. 12. The error is reduced to 3.6% maximum at $I_{FC} = 6$ A, and the error at $I_{FC} = 0$ A is almost 0%.

The internal current component only influences the behavior of the steady state in the activation polarization region. In the higher current region, the influence of the internal impedance (R^{int}) of the fuel cell becomes higher, while the influence of the activation polarization diminishes.

4.3. Step-response verification

The verification of the step-response is done in two ways. First, the error plot of the step-response presented in Fig. 10 is simulated with Matlab with an open circuit voltage source without internal current term (I_n). The top graph of Fig. 13 shows the relative error as defined in (14) between measurement and simulation. The alternative, an open circuit voltage source (E_{FC}) with I_n, is shown in the bottom graph of Fig. 13.

The error of the step-response is highly dependent on the open circuit voltage source. As is seen in Fig. 13, the internal

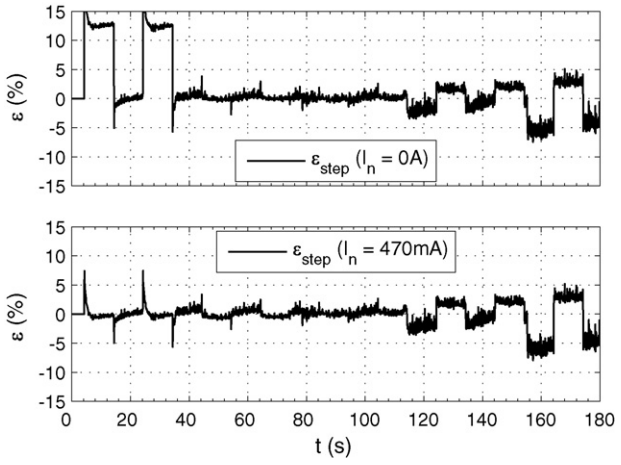

Fig. 13. Relative error between the measured and simulated step characteristics. In the top figure, the FC voltage is simulated without internal current, while in the bottom figure it is simulated with internal current.

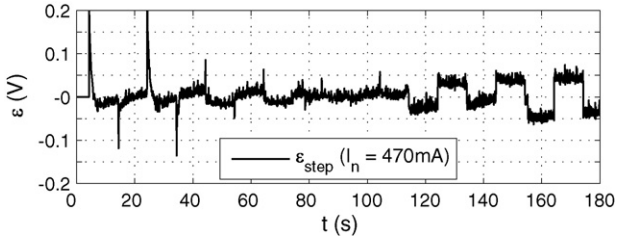

Fig. 14. Absolute error between the measured and simulated step characteristics.

current term in the steady-state characteristic (15) influences the large-signal behavior, especially in the low output current region (activation polarization). It can also be seen in Fig. 13 that the errors of the large-signal behavior at $I_{FC} = 6$ A, that is the steps in the time interval $155 < t < 180$, are higher when the internal current is included than without this term. This is also related to the error in the steady-state behavior, as can be seen in Fig. 12.

The difference in absolute value between the simulated voltage and the measured characteristic is very small over the complete current range, as is shown in Fig. 14. However, the error in the higher current range increases relatively more because of a lower fuel cell output voltage, as can be seen in Figs. 10 and 14.

The large peak errors in the activation polarization region seen in Figs. 13 and 14, are caused due to instantaneous changing of the resistor values as a result of a different load current. In practice, the change in resistance will not be so abrupt. The peaks have a limited duration of only a couple of microseconds.

5. Conclusions

This paper provides a way of constructing an accurate fuel cell model based on electrochemical phenomena. The model is constructed as an equivalent circuit model, and is capable of simulating the static and dynamic behavior of PEM fuel cells, a so-called dynastatic model.

The results obtained from electrochemical impedance spectroscopy are used to find the small-signal behavior. From the EIS data the values of the resistor parameters can be found, together with a first indication for the capacitors and inductor values of the third-order equivalent circuit. The two double layer resistors (R_{DL} and R_R) are non-linearly dependent on the output current (I_{FC}). The bulk resistor (R_∞) may be assumed constant and the adsorption resistor (R_A) is linearly dependent on the output current.

Once the internal resistance is known, the open circuit voltage source (E_{FC}) of the equivalent circuit can be retrieved. In order to reduce the simulation error at no load, an estimation of the internal current (I_n) of the fuel cell is introduced. The additional internal current parameter is not only necessary to reduce the steady-state error, but also to reduce the error in the step-response.

Finally, the indicative values of the capacitors and inductor from EIS can be used to find the optimal values with respect to the step-response measurements. When the capacitors and inductor values are fitted, the dynastatic model is complete.

The fuel cell model is characterized by performing small-signal, steady-state and large-signal measurements. Because the modeling approach fully relies on these measurement results, electrochemical phenomena like temperature dependency, charge double layer and adsorption effects are implicitly covered with the current dependent element values.

Acknowledgements

The authors would like to thank Marijn Uyt de Willigen and Wim Thirion for their assistance in producing the test-setup and for their efforts during the measurements. Furthermore, the authors thank Marcel Geers, who worked for his practical training on some of the presented measurement results.

References

[1] U.S. Department of Energy, Fuel Cell Handbook, fifth ed., EG&G Services, Morgantown, 2000.
[2] J.C. Amphlett, R.M. Baumert, R.F. Mann, B.A. Peppley, P.R. Roberge, J. Electrochem. Soc. 142 (1) (1995) 1–15.
[3] R.F. Mann, J.C. Amphlett, J.C. Hooper, H.M. Jensen, B.A. Peppley, P.R. Roberge, J. Power Sources 86 (1–2) (2000) 173–180.
[4] J.C. Amphlett, R.F. Mann, B.A. Peppley, P.R. Roberge, A. Rodrigues, J. Power Sources 61 (1996) 183–188.
[5] M.W. Fowler, R.F. Mann, J.C. Amphlett, B.A. Peppley, P.R. Roberge, J. Power Sources 106 (1–2) (2002) 274–283.
[6] J.H. Lee, T.R. Lalk, J. Power Sources 73 (2) (1998) 229–268.
[7] D. Chu, R. Jiang, C. Walker, J. Appl. Electrochem. 30 (3) (2000) 365–370.
[8] J. Larminie, A. Dicks, Fuel Cell Systems Explained, John Wiley & Sons Ltd, Chichester, 2001.
[9] P.J.H. Wingelaar, J.L. Duarte, M.A.M. Hendrix, 2005 IEEE Power Electronics Specialists Conference, 2005.
[10] P.J.H. Wingelaar, J.L. Duarte, M.A.M. Hendrix, 2006 IEEE International Symposium on Industrial Electronics, 2006.
[11] K. Wippermann, A.A. Kulikovsky, H. Schmitz, J. Mergel, B. Fricke, T. Sanders, D.U. Sauer, Grundlagen zur Impedanzspektroskopie an Brennstoffzellen und ortsaufgel0ste Messungen, Impedanzspektroskopie, Grundlagen und Anwendungen 2006, 2005, pp. 96–106.

[12] G. Fontes, C. Turpin, R. Saisset, T. Meynard, S. Astier, 2004 35th Annual IEEE Power Electronics Specialists Conference, 2004, pp. 4729–4735.
[13] J. Ross Macdonald (Ed.), Impedance Spectroscopy, Emphasizing Solid Materials and Systems, John Wiley & Sons Ltd, New York, 1987.
[14] J.T. Muller, P.M. Urban, W.F. Holderich, J. Power Sources 84 (1999) 157–160.
[15] L. Bai, B.E. Conway, Electrochim. Acta 38 (14) (1993) 1803–1815.
[16] V.S. Bagotsky (Ed.), Fundamentals of Electrochemistry, John Wiley & Sons Inc., Hoboken, New Jersey, 2006.
[17] W.A. Fuglevand, S.I. Bayyuk, G.A. Lloyed, P.D.De Vries, D.R. Lott, J.P. Scartozzi, M. Somers, R.G. Stokes, U.S. Patent: 6 218 035, 2001.
[18] W.A. Fuglevand, P.D.De Vries, G.A. Lloyed, D.R. Lott, J.P. Scartozzi, U.S. Patent: 6 096 449, 2000.